Revealing the Interface in Polymer Nanocomposites

Mauro Zammarano,[†,‡,§,*] Paul H. Maupin,[⊥] Li-Piin Sung,[‡] Jeffrey W. Gilman,[§] Edward D. McCarthy,[§] Yeon S. Kim,[‡] and Douglas M. Fox[†]

[†]Department of Chemistry, American University, Washington, DC 20016, United States, [‡]Engineering Laboratory, and [§]Material Measurement Laboratory, National Institute of Standards and Technology (NIST), 100 Bureau Drive, Gaithersburg, Maryland 20899-8665, United States, and [⊥]Chemical Sciences, Geosciences, and Biosciences Division Office of Basic Energy Sciences, U.S. Department of Energy, Washington, DC 20585-1290, United States

ABSTRACT The morphological characterization of polymer nanocomposites over multiple length scales is a fundamental challenge. Here, we report a technique for high-throughput monitoring of interface and dispersion in polymer nanocomposites based on Förster resonance energy transfer (FRET). Nanofibrillated cellulose (NFC), fluorescently labeled with 5-(4,6-dichlorotriazinyl)-aminofluorescein (FL) and dispersed into polyethylene (PE) doped with Coumarin 30 (C30), is used as a model system to assess the ability of FRET to evaluate the effect of processing on NFC dispersion in PE. The level of energy transfer and its standard deviation, measured by fluorescence spectroscopy and laser scanning confocal microscopy (LSCM), are exploited to monitor the extent of interface formation and composite homogeneity, respectively. FRET algorithms are used to generate color-coded images for a real-space observation of energy transfer efficiency. These images reveal interface formation at a nanoscale while probing a macroscale area that is large enough to be representative of the entire sample. The unique ability of this technique to simultaneously provide orientation/spatial information at a macroscale and nanoscale features, encoded in the FRET signal, provides a new powerful tool for structure–property-processing investigation in polymer nanocomposites.

KEYWORDS: nanocomposite · interface · fluorescence · FRET · confocal microscopy

One of the most enduring problems in the evolution of science and technology using nanoscale materials is the characterization of their morphology in macroscopic systems.[1−3] This involves spatial and orientation distribution, which may be multimodal and hierarchical, and requires information from the nano- to the macroscale, that is, over 6 orders of magnitude in length scale. Several techniques have been developed for character izing the morphology of polymer nanocomposites, but none of them is a stand-alone method, capable of addressing all of these requirements simultaneously; thus, a multitude of techniques is generally necessary.

According to Vaia *et al.*,[4] characterization methods can be categorized into four groups: (1) real-space observations that allow a direct morphological observation (*e.g.*, optical,[5] transmission,[6] and scanning electron microscopy);[7] (2) macroscopic property measurements that require a theoretical response model and provide indirect morphological information (*e.g.*, rheology);[8] (3) physical response measurements that are directly related to the amount of interfacial area (*e.g.*, nuclear magnetic resonance[9] and fluorescence);[10,11] (4) reciprocal space observations based on scattering that provide a bulk measurement of alignment and dispersion (*e.g.*, X-ray,[4,6] light,[12] and neutron scattering).[13] The most widely used of these methods is transmission electron microscopy (TEM) that requires time-consuming sample preparation (*i.e.*, microtoming) and the acquisition of tens of micrographs with statistical analysis of data to provide a representative view of nanocomposite structure.[6] Solid-state nuclear magnetic resonance can quantitatively measure the extent of dispersion but requires paramagnetic nanoparticles, deoxygenated samples (for quantitative measurement only), sophisticated instrumentation, which may not be readily available, and is also a bulk measurement that does not provide spatial and orientation information.[9] Fluorescence methods have been used to characterize the dispersion of layered silicates and carbon nanotubes in polymer nanocomposites.[10,11] Previous studies in fluorescence microscopy and resonance energy transfer in imaging cellulose fiber interfaces[14] indicate the potential for the exploration of nonmicroscopically based systems in the development of readily available online characterization methods. Laser scanning confocal microscopy (LSCM) is used as a high-throughput technique capable of visualizing the morphology of a nanocomposite in three dimensions with minimal sample preparation; however, it does not provide nanoscale resolution.[12,15] The coupling of photochemistry or photophysics to microscopy has great promise for agile characterization of nanoscale systems.[16−18]

* Address correspondence to mzam@nist.gov or zammarano@gmail.com.

Received for review November 1, 2010 and accepted March 16, 2011.

Published online March 16, 2011
10.1021/nn102951n

In a polymer composite, the properties of the polymer region near the reinforcing agent, the so-called interface, are different from those of the bulk.[19] There is evidence that such an interface zone must be included in models in order to represent the overall composite properties.[20] This is particularly important in polymer nanocomposites, where the volume fraction of the interface region constitutes a significant volume fraction of the composite even at low filler concentrations.[3] In all cases, the interface between the composite components plays a defining role in the overall material properties such as glass transition temperature,[17,21] relaxation dynamics,[22,23] aging,[24] dielectric behavior (*i.e.*, breakdown strength, voltage endurance, and dielectric permittivity),[25] density,[26] mechanical properties (*i.e.*, stiffness, debonding, fracture, internal stress distribution, and toughness),[20,26] and flammability.[27] The measurement of the interface volume fraction is, therefore, pivotal for structure−property-processing investigation and modeling of polymer nanocomposites.

Here, we show how Förster resonance energy transfer (FRET) combined with spectroscopic analysis or LSCM can be used to monitor interface formation at the nanoscale through an easily accessible method that is amenable to high-throughput testing. FRET is a process by which a fluorophore (the donor), in an excited state, transfers its energy to a neighboring molecule (the acceptor) by nonradiative dipole−dipole interaction.[28,29] The energy transfer efficiency between a donor and acceptor at a distance R decreases sharply with R: it is equal to 50% for $R = R_0$ (where R_0 is the Förster distance) by definition and drops to about 1% for $R = 2R_0$. Typical values of R_0 are between 2 and 6 nm, thus the FRET efficiency is typically negligible for $R >$ 10 nm.[30] In a composite, where both the reinforcing phase and the matrix are fluorescently labeled, FRET occurs only at a distance of a few nanometers from the interface, revealing the interface itself. This implies that FRET can encode nanofeatures (*i.e.*, extent of interface formation) in optical microscopy, which are beyond the resolution limit of optical microscopy (Abbe limit).[31] By combining optical microscopy techniques (*e.g.*, LSCM) with FRET, one can probe an area that is large enough to be representative of the entire sample (macroscale) and still retain information at a smaller scale (nanoscale) which is intrinsically encoded in the FRET signal. This is a major advantage over standard microscopy, where there is a trade-off between resolution/magnification and the ability to display macroscale features that are important from an engineering point of view. Multiscale characterization of the hierarchical structure in nanocomposites is critical for the realization of these systems.[4,32]

As a proof-of-concept system, we use nanofibrillated cellulose (NFC)[33,34] that is fluorescently labeled with 5-(4,6-dichlorotriazinyl)aminofluorescein (FL) and dispersed into polyethylene (PE), doped with Coumarin 30 (C30). The effect of processing on NFC dispersion is monitored by measuring the extent of energy transfer with fluorescence spectroscopy. In addition, FRET combined with LSCM (FRET/LSCM for the remainder) can provide a real-space observation for interface formation in polymer nanocomposites by generating energy-transfer-efficiency maps.

FRET/LSCM has near-term applications for assessing the structure−property-processing relations governing polymer nanocomposites, such as optimization of processing parameters and surface modifiers selection, nondestructive testing for monitoring polymer−fiber debonding, correlation between crack formation and interface distribution at a macroscale, correlation between the viscoelastic response (as measured, for example, by nanoindentation or atomic force microscope) and interface distribution.

RESULTS AND DISCUSSION

A proof-of-concept system was realized by varying the extent of dispersion of NFC labeled with FL (FLNFC) in PE containing C30. The proper labeling of NFC with FL in FLNFC (*i.e.*, complete and homogeneous labeling of NFC without losing nanofibrillation) was verified by LSCM and scanning electron microscopy (SEM). LSCM images of the same selected area were collected both in reflection mode (488 nm excitation laser, no filter) to collect all reflected light and fluorescence mode (488 nm excitation laser, 505 nm low pass filter) to collect only the fluorescence emitted by FLNFC (Figure 1A,B). The image generated by reflected mode shows the identical features to the image generated by fluorescent mode. Nanofibrils with a diameter of about 100 nm can be observed in fluorescent mode, and no aggregate of self-quenched FL is observed in reflection mode. SEM micrographs (Figure 1C,D) show that the morphology of the NFC surface is not affected by the labeling process and nanofibrils are still present after labeling.

The basic principle used for revealing the cellulose−polymer interface is illustrated in Figure 2. FLNFC has an absorption peak at a wavelength (λ^A_{abs}) of about 497 nm and an emission peak (λ^A_{em}) at a wavelength of about 527 nm, as measured by UV−vis−NIR and fluorescence spectroscopy, respectively. Similarly, C30 has a $\lambda^D_{abs} \approx 407$ nm and $\lambda^D_{em} \approx 493$ nm. There is a significant spectral overlap between the emission of C30 (donor) and the absorption of FLNFC (acceptor). As previously described, FRET will occur only if the distance between donor and acceptor is in the range of a few nanometers. This means that FRET occurs at the interface, where donor and acceptor are in close proximity but does not occur for isolated acceptors or donors in the composite (Figure 2).

In addition, a higher extent of dispersion of the reinforcing phase (FLNFC) will generate an increase in interface and FRET. Two different levels of dispersion

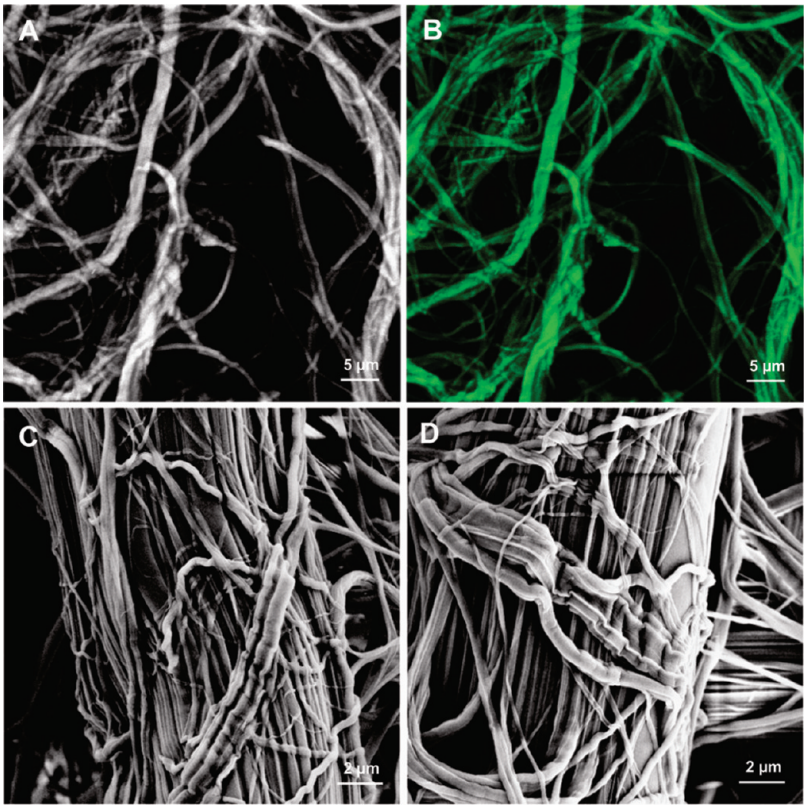

Figure 1. (A) LSCM image of nanofibrillated cellulose labeled with reactive fluorescein in reflection mode (458 nm excitation laser, no filter) and (B) in fluorescence mode (458 nm excitation laser, 505 nm low pass filter). (C) SEM micrograph of nanofibrillated cellulose before labeling and (D) after labeling.

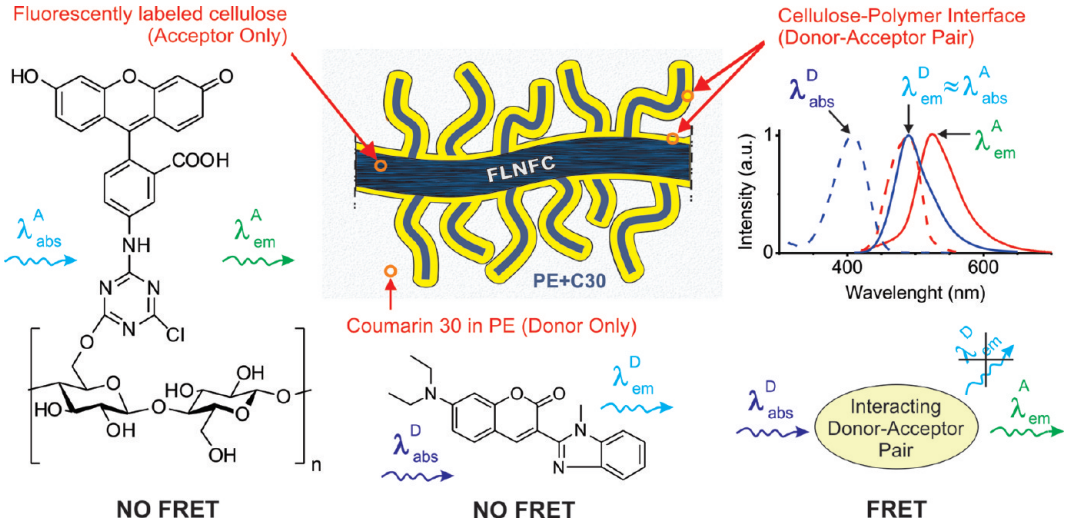

Figure 2. Schematic drawing illustrating the use of FRET for revealing the interface in polymer composites. FRET occurs only at the cellulose–polymer interphase where interacting donor–acceptor pairs are formed. The normalized spectra of the absorption (dashed line) and the emission (solid line) for the acceptor and donor are also shown.

of FLNFC in PE were achieved by using two grades of FLNFC: pristine FLNFC, with a low bulk density, and FLNFC in a preagglomerated prill form (FLNFCp). (Preagglomerated prills are commonly used to increase feeding speed of low-density natural fibers during extrusion.) PE was extruded with both types of fibers at the same processing conditions. Formulations of samples with their identification names and fluorescence data are shown in Table 1. A representative emission spectrum for each sample is shown in Figure 3. PE-NFC (no fluorophore) is a control sample used for background correction. PE-FLNFC is the acceptor-only sample. The excitation wavelength used here (black-light) is capable of efficiently exciting the donor (C30) but not the acceptor (FLNFC). The acceptor-only sample (PE-FLNFC) shows a relatively weak

TABLE 1. Sample Formulations and Normalized Fluorescence Intensities[a]

		fluorescence			
		peak 1		peak 2	
sample id	additive	wavelength (nm)	intensity (au)	wavelength (nm)	intensity (au)
PE-NFC	NFC				
PE-C30	C30	493.2 ± 0.2	1.00 ± 0.03		
PE-C30 +NFC	C30 + NFC	495.5 ± 0.2	0.68 ± 0.02		
PE-C30 + NFCp	C30 + NFCp	493.8 ± 0.4	0.83 ± 0.02		
PE-FLNFC	FLNFC			526.7 ± 0.0	0.12 ± 0.00
PE-C30 + FLNFC	C30 + FLNFC	495.6 ± 0.3	0.53 ± 0.01	519.2 ± 0.2	0.47 ± 0.02
PE-C30 + FLNFCp	C30 + FLNFCp	494.0 ± 0.6	0.66 ± 0.05	524.5 ± 2.1	0.57 ± 0.01

[a] The data shown here are the average of at least five replicates. The standard deviation (σ) is also reported. NFC: pristine unlabeled nanofibrillated cellulose fibers. NFCp: unlabeled NFC in a prill form. FLNFC: fluorescently labeled NFC. FLNFCp: fluorescently labeled NFC in a prill form.

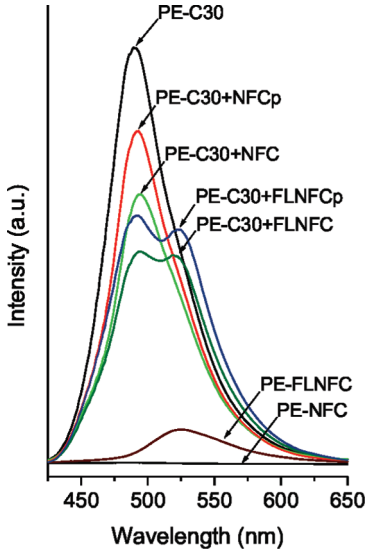

Figure 3. Representative fluorescence spectra for samples of Table 1. The presence of FLNFC reduces C30 fluorescence due to FRET and scattering/absorption.

fluorescence peak at about 527 nm due to bleed-through in excitation (*i.e.*, the direct excitation of the acceptor at the donor excitation wavelength),[35] but the donor−acceptor samples (PE-C30 + FLNFC and PE-C30 + FLNFCp) show an evident increase in acceptor fluorescence at the same wavelength due to FRET. The donor-only sample (PE-C30) has an intense fluorescent peak (1.00 au) at about 493 nm. The presence of unlabeled cellulose fibers decreases the donor peak intensity (0.83 au for PE-C30 + NFCp and 0.68 au for PE-C30 + NFC) due to scattering and absorption.[36] NFC is much more homogeneously dispersed than NFCp (see LSCM data below), and the fluorescence intensity (for both donor and acceptor) progressively decreases with the increase in dispersion of the cellulose fibers, due to light scattering. In addition, a FRET-induced reduction in donor fluorescence is observed in the presence of the labeled cellulose fibers (0.66 au for PE-C30 + FLNFCp and 0.53 au for PE-C30 + FLNFC).

In a donor−acceptor sample, the ratio of the acceptor-to-donor peak (ρ) is a function of FRET and the concentration of fluorescently labeled cellulose.[38] For a perfectly homogeneous dispersion, ideally, ρ should be constant throughout the sample and increase with the extent of dispersion. However, in practice, heterogeneity due to variations in concentration and energy transfer efficiency will affect ρ. An increase in the extent of interfacial surface area will induce an increase in the mean value of ρ measured for a given sample (ρ_{ave}). The ρ_{ave} is an index of interfacial surface area, whereas its standard deviation (σ) is an index of sample heterogeneity.

A relative noise ($2\sigma/\rho_{ave}$) can be calculated for monitoring the quality of dispersion as a ratio of the heterogeneity over interfacial surface area index: a lower relative noise implies a more homogeneous and higher interfacial surface area in the sample. A relative noise measurement was previously used for proving the ability of LSCM to assess the dispersion of carbon nanotubes in polystyrene.[37] The relative noise can be profitably used as a dispersion index as shown by the values calculated for samples PE-C30 + FLNFC ($2\sigma/\rho_{ave}$ = 0.03) and PE-C30 + FLNFCp ($2\sigma/\rho_{ave}$ = 0.16). Note that the ρ value measured for each sample is already averaged over the observed area by the fiber optic of the spectrometer. Herein, the sample-to-probe distance was fixed at 10 mm; however, this distance can be easily tuned in order to adjust the observed area to the extent of dispersion of the sample: the more homogeneous the sample is, the lower the sample-to-probe distance can be in order to observe an area that is representative of the entire sample. This spectroscopic approach provides a simple bulk method for qualitative assessment of dispersion and homogeneity in polymer nanocomposites, suitable for online and *in situ* analyses (*e.g.*, during extrusion or reaction).

Further insights on dispersion and interface formation can be achieved by means of FRET/LSCM with sensitized emission (donor and/or acceptor fluorescence intensity measurement with direct donor excitation) and

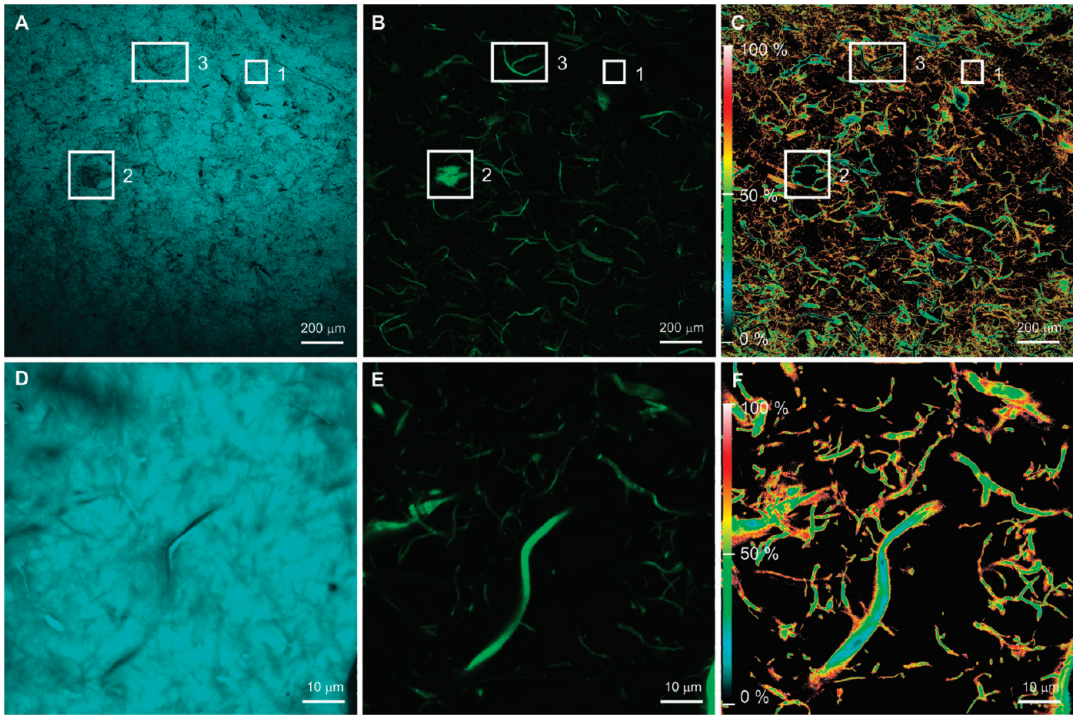

Figure 4. FRET/LSCM false-color images for PE-C30 + FLNFC: (A) C30 fluorescence (donor filter set) at 5× magnification; (B) FLNFC fluorescence (acceptor filter set) at 5×; (C) energy-transfer-efficiency map calculated according to the N_{FRET} algorithm at 5× (N_{FRET} = 0.121); (D) C30 fluorescence at 100×; (E) FLNFC fluorescence at 100×; (F) energy-transfer-efficiency map at 100×.

TABLE 2. FRET Indexes Calculated for PE-C30 + FLNFCp and PE-C30 + FLNFC at 5× Magnification[a]

	FRET index		
sample	FRETN × 10^2 (σ %)	*nF* × 10^2 (σ %)	N_{FRET} × 10^2 (σ %)
PE-C30 + FLNFCp	0.20 (27.6)	−0.38 (−159.0)	1.81 (51.4)
PE-C30 + FLNFC	1.95 (12.7)	3.41 (7.0)	12.2 (2.5)

[a] The data shown here for each index are the averages of five replicates. The relative standard deviation (σ %), calculated as a percentage of the ratio of the standard deviation to the average value of the FRET index, is also reported.

acceptor photobleaching (donor fluorescence intensity measurement with donor direct excitation before and after acceptor photobleaching).[35] The acceptor photobleaching approach was exploited only to conceptually support the occurrence of FRET, and it is further discussed in Supporting Information (Figure S1).

Representative FRET/LSCM images in sensitized emission mode for PE-C30 + FLNFC and PE-C30 + FLNFCp are shown in Figure 4 and Figure 5, respectively. They show donor, acceptor fluorescence, and energy-transfer-efficiency map calculated by FRET analysis at 5× and 100× magnification. High-resolution images of Figure 4 and Figure 5 plus additional images from the FRET filter set are shown in Supporting Information (Figures S2−S5).

Large aggregates of FLNFC are observed with the acceptor filter set (Figure 5B) for PE-C30 + FLNFCp, whereas a more homogeneous dispersion is observed for PE-C30 + FLNFC (Figure 4B). The donor filter set (Figure 5A, inset box 1) shows that there is no significant fluorescence in the areas where the fiber aggregates are localized (a residual weak fluorescence is generated by the acceptor fluorescence due to cross-talk). This demonstrates that the hydrophobic C30 does not diffuse into the hydrophilic aggregates of cellulose fibers. In such a system, a fluorescein dye molecule that is located just few nanometers inside an aggregate of cellulose fibers is not contributing to FRET. An increase in the extent of dispersion of the reinforcing phase (FLNFC) will expose more fluorescein molecules at the cellulose−polymer interface and induce an increase in FRET.

A FRET index is a relative value of energy transfer efficiency that changes with the donor−acceptor configuration. There are a variety of FRET indexes that have been developed.[35] In the present work, we exploited FRET indexes calculated according to three different algorithms: N_{FRET} (Xia *et al.*[38]), FRETN (Gordon *et al.*[39]), and *nF* (Youvan *et al.*[40]). These algorithms were applied pixel by pixel to the three-channel confocal images to generate energy-transfer-efficiency maps (*e.g.*, Figures 4C,F and 5C,F). An average value of FRET index was calculated for each map. Five different maps per sample were used to calculate an average and standard deviation for each FRET index at 5× magnification. Table 2 shows the average and standard deviation

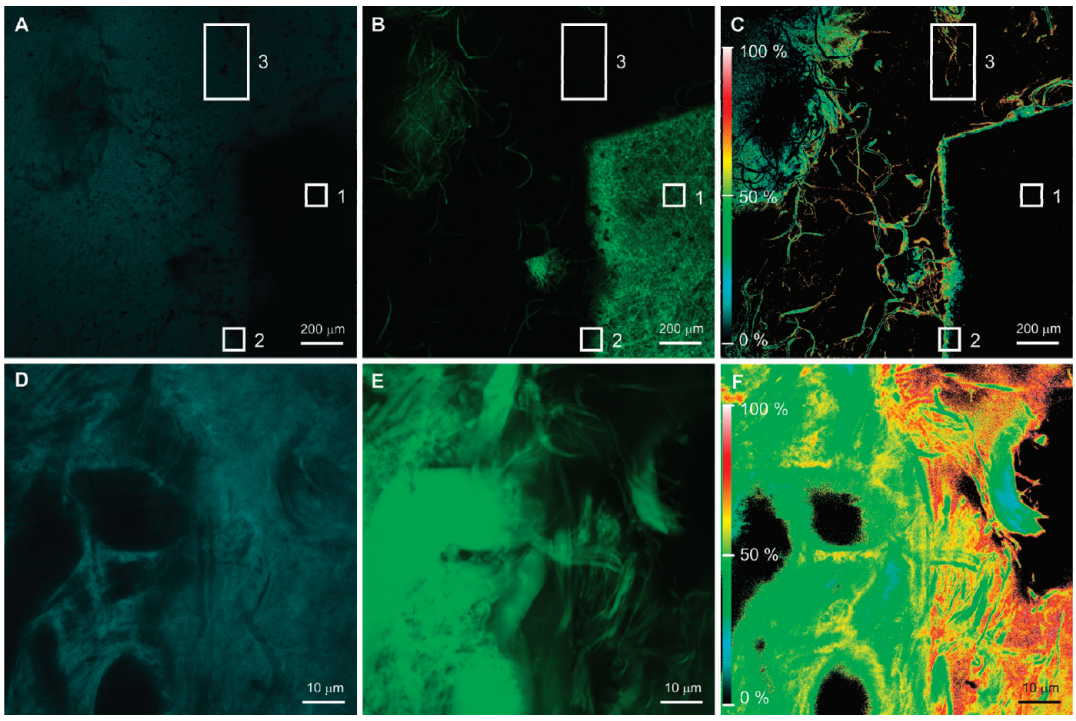

Figure 5. FRET/LSCM false-color images for PE-C30 + FLNFCp: (A) C30 fluorescence (donor filter set) at 5× magnification; (B) FLNFC fluorescence (acceptor filter set) at 5×; (C) energy-transfer-efficiency map calculated according to the N_{FRET} algorithm at 5× (N_{FRET} = 0.010); (D) C30 fluorescence at 100×; (E) FLNFC fluorescence at 100×; (F) energy-transfer-efficiency map at 100×.

values of each index for the samples PE-C30 + FLNFC and PE-C30 + FLNFCp.

As expected, the more homogeneously dispersed sample (PE-C30 + NFC) shows an increase of all three indexes as compared to PE-C30 + NFCp, due to an increase in interface. The negative values of *nF* for PE-C30 + NFCp suggest that this index is not adequate for poorly dispersed samples due to extreme variations in acceptor and donor concentrations that are not corrected in this algorithm.[40] FRETN and N_{FRET} provide, instead, index values which are normalized by the donor−acceptor concentrations. FRETN and N_{FRET} show approximately a 10- and 7-fold increase, respectively, between PE-C30 + FLNFCp and PE-C30 + FLNFC.[38] In particular, N_{FRET} is the most reliable index in systems where there are large local variations in the donor-to-acceptor concentration ratio. Compared to all other indexes, N_{FRET} has the smallest variation (σ % = 2.5) for PE-C30 + FLNFC and the highest variation (σ % = 51.4) for PE-C30 + FLNFCp. This suggests that at this magnification (5×) the scanned area is sufficient to represent the extent of dispersion for PE-C30 + FLNFC and capture the large variations in dispersion and fiber concentration for PE-C30 + FLNFCp. Note that at higher magnification (*e.g.*, 100×) the observed area (84 μm × 84 μm) is comparable in size to the residue aggregates (inset box 2, Figure 4) and, thus, it is not representative of the extent of dispersion for PE-C30 + FLNFC.

Figures 4C,F and 5C,F show the energy-transfer-efficiency map calculated according to the N_{FRET} algorithm for PE-C30 + FLNFC and PE-C30 + FLNFCp. These are color-coded images generated for real-space observation of energy transfer efficiency that reveal interface formation at a nanoscale while probing a macroscale area that is large enough to be representative of the entire sample. The actual spatial resolution of these energy-transfer-efficiency maps is the same as that for LSCM. However, information about interface formation at the nanoscale, which is not resolvable by LSCM, is encoded in the FRET signal (*i.e.*, the calculated energy transfer efficiency for each pixel is dependent on the actual extent of interface formation). This means that this technique provides a powerful tool for morphological characterization of polymer nanocomposites by merging information over 6 orders of magnitude in length scale: (1) extent of interface formation at a nanoscale; (2) orientation/spatial information at meso- and macroscale. In this study, we used only two-dimensional images; however, in principle, a three-dimensional FRET analysis might also be carried out, in fact, LSCM can generate a three-dimensional visualization of nanocomposites through optical sectioning.[12]

Inset box 2 in Figure 5 illustrates, as speculated, that FRET is occurring at the polymer−cellulose interface and not inside aggregates of NFC (see inset box 1 of Figure 5 and inset box 2 of Figure 4) because C30 is not able to penetrate them. Even if small aggregates (≈100 μm) are still present in PE-C30 + FLNFC (*e.g.*, inset box 2 of Figure 4), the higher extent of dispersion induces a

one order of magnitude increase in the polymer−cellulose interface. The N_{FRET} value (average calculated over the entire image) is 0.121 for Figure 4C and 0.010 for Figure 5C.

NFC can be considered as a hybrid nano/micro reinforcing agent with microfeatures (*i.e.*, the core microfibers) and nanofeatures (*i.e.*, the protruding nanofibrils). The microfibers can be easily detected by FRET mapping (Figure 4C, inset box 3). Nanofibrils on NFC, with a diameter between 50 to 500 nm, are beyond the resolution limit of LSCM at 5× magnification (Abbe limit of about 1.5 μm). Nevertheless, their contribution to interface formation is predominant as compared to the core microfibers, due to their intrinsically high surface area. This may explain why, in the areas where the highest energy transfer efficiency is reached, no NFC can be observed with the acceptor filter set (*e.g.*, Figure 4, inset box 1). A further proof of this concept comes from the comparison of inset box 2 across Figure 5. On activation of FRET visualization in Figure 5C, there is the sudden appearance of a strong FRET signal in an area previously devoid of fluorescence, immediately to the left of the apparent edge of the aggregate visible in Figure 5B. A similar trend is apparent throughout the image. Figure 5D−F shows the interface region magnified by 100× (Abbe limit of about 150 nm) and confirms that energy transfer occurs predominantly at the nanofibril−polymer interface. This suggests that this technique is even more interesting for composites containing fully nanoreinforcing agents (*e.g.*, tunicin),[41] which are able to create significantly more polymer−filler interface than NFC does.

Figure 4D−F shows a representative area for PE-C30 + FLNFC at 100×. Isolated microfibers and nanofibrils are observed. This means that FLNFC splits into its component parts during compounding, most likely due to severe shearing. SEM micrographs (Figure 6) provide further insights into the effect of shearing on the morphology of FLNFC. Bundles of fibers with a diameter up to 10 μm are observed before extrusion, whereas a very homogeneous dispersion of fibers with a typical diameter of about 1 μm is observed after extrusion. Thus, compounding is also promoting debundling and inducing a reduction in the average diameter of the fibers.

Note that SEM does not provide a representative view of the composite structure even at the relatively low magnification of Figure 6B. Small aggregates (~100 μm) are evident by FRET/LSCM (inset box 2 of Figure 4), but they are not obvious by SEM. This example shows that, contrary to standard microscopy (*e.g.*, transmission/scanning electron microscopy and optical microscopy) where an intrinsic trade-off exists between resolution and accurately representing the average dispersion, FRET/LSCM can capture an image that is representative of the entire sample in terms of dispersion while still retaining nanoscale information, encoded in the FRET signal. The resolution gap between electron microscopy and FRET/LSCM is substantially reduced by new super resolution fluorescence microscopy.[42,43]

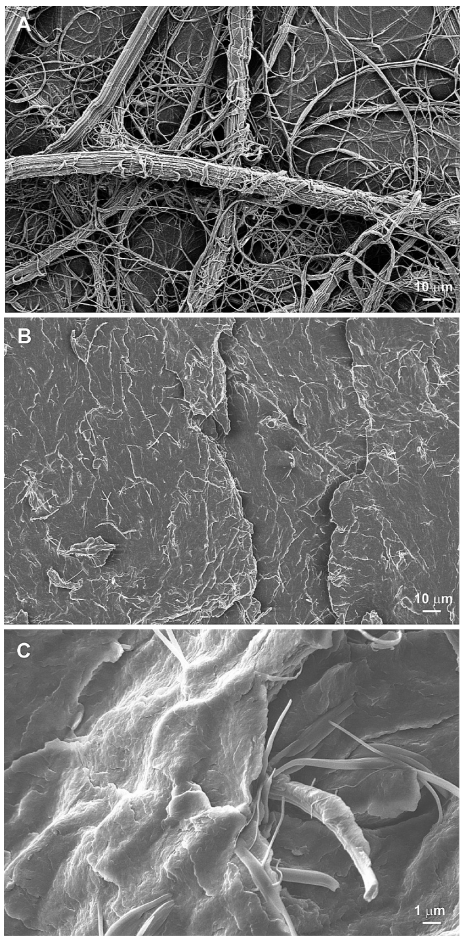

Figure 6. SEM micrographs for (A) FLNFC before compounding; (B) FLNFC on cryo-fractured PE-C30 + FLNFC at low magnification and (C) high magnification.

CONCLUSIONS

The results presented here demonstrated that FRET can be used to monitor the extent of interface formation in polymer nanocomposites by (a) a simple spectroscopic approach for a qualitative bulk assessment of dispersion and homogeneity, suitable for online and *in situ* analyses; (b) using LSCM to obtain real-space observation of interface formation based on energy-transfer-efficiency maps. FRET encodes nanofeatures (*i.e.*, extent of interface formation) in optical microscopy (*e.g.*, LSCM), which are beyond the resolution limit of optical microscopy (Abbe limit). FRET/LSCM can probe an area that is large enough to be representative of the entire sample (macroscale) and still present information at a smaller scale (nanoscale) which is intrinsically encoded in the FRET signal. This is a major advantage over standard microscopy, where there is a trade-off between

resolution/magnification and the ability to display macroscale features that are important from an engineering point of view. In particular, FRET/LSCM provides a powerful tool with unique features for the morphological characterization of polymer nanocomposites across many length scales, such as (1) nanoscale information about interface formation based on FRET; (2) meso- and macroscale information with orientation and spatial information based on LSCM three-dimensional visualization; (3) more readily accessible instrumentation than other techniques; and (4) minimal sample preparation. Limitations of this method are that fluorescently labeled samples are required and that fluorescence might be affected by the processing conditions.

METHODS

Materials. NFC, Lyocell L040-6 with a precursor length of 6 mm and nanofibrils with a diameter between 50 and 500 nm, was obtained from Engineered Fibers Technology (Shelton, CT). Fluorescent dyes, Coumarin 30 (C30), and 5-(4,6-dichlorotriazinyl)aminofluorescein (FL) were purchased from Sigma-Aldrich (Milwaukee, WI) and Invitrogen (Carlsbad, CA), respectively. Medium density polyethylene (PE), with $M_n \approx 1800$ and a density of 0.94 g/cm^3, was supplied by Scientific Polymer Products (Ontario, NY). Sodium hydroxide pellets were purchased from Aldrich. Deionized water (18.3 MΩ) was used throughout sample preparation. (According to ISO 31-8, the term "molecular weight" has been replaced by "relative molecular mass", symbol M_r. Thus, if this nomenclature and notation were to be followed in this publication, one would write $M_{r,n}$ instead of the historically conventional M_n for the number average molecular weight. The conventional notation, rather than the ISO notation, has been employed for this publication.)

Sample Preparation. NFC was purified by thoroughly washing with water and then labeled with FL using a method similar to the one previously reported by Helbert *et al.*[44] Briefly, NFC (5.00 g) and FL (0.12 g) were added into 800 and 200 mL, respectively, of 0.51 N NaOH. The two solutions were first stirred separately for 40 min, and then combined together and stirred for 4 days at room temperature. The suspension was repeatedly washed with water on a filter paper (2.5 μm pore size, 24 cm diameter; Whatman, UK), until the filtrate showed an electrical conductivity of 2.5 μS and no residual fluorescence, at which point it was dried at 80 °C. Densified fiber prills of NFC were prepared by pressing the fibers (3.4 GPa, room temperature). PE composite samples (4 g) were prepared by extrusion in a microcompounder (DACA Instruments, Santa Barbara, CA) at a temperature of 108 °C and with a residence time of 5 min. A concentrated batch containing 2% by mass of C30 in PE was prepared and then re-extruded with neat PE to obtain samples with 0.19% by mass of C30 and/or 5% by mass of NFC, NFCp, FLNFC or FLNFCp. A control sample containing only 5% by mass of NFC in PE was also prepared. The extrusion time and temperature were identical for all of the samples to prevent any difference in fluorescence induced by thermal degradation or oxidation. The polymeric blends were hot-pressed at 115 °C for 2 min to obtain disk-shaped samples (diameter 14 mm, thickness 1.2 mm) in a Carver press (model #3912) and cooled *in situ* with a forced air flow system. A Kapton polyimide film was used to prevent the adhesion of the material to the metallic mold.

Fluorescence Spectroscopy. Fluorescence spectra were obtained using an Ocean Optics USB2000 spectrometer adapted for fiber optic input with a 200 μm entrance slit width. The fiber-optic input was placed normal to the sample at a distance of 10 mm. The excitation source was a 30 W black-light at 365 nm placed at about 3 cm from the sample. Fluorescent spectra were collected with an integration time of 15 ms and averaged over 100 replicas to correct variations due to fluctuations of the lamp intensity. The final emission spectra were background corrected, smoothed, and finally normalized by dividing by the average peak intensity of PE-C30. All measurements were made at room temperature.

UV–Vis. The absorption spectra were collected in a quartz cuvette by a UV–vis–NIR (Perkin-Elmer Lambda 950) spectrometer for FLNFC in water suspension and C30 dissolved in acetonitrile. Data were recorded at 1 nm increments.

LSCM. A confocal laser scanning microscope (LSM 510 META Carl Zeiss, Germany) was used to detect FRET. The primary beam splitter was dichroic (405 and 488 nm). The donor filter setup consisted of an excitation source (405 nm diode laser, 30 mW) and emission band-pass filter (420 to 480 nm). The acceptor setup consisted of an excitation source (488 nm argon laser, 30 mW) and emission band-pass filter (505 to 550 nm). The FRET filter setup consisted of an excitation source (405 nm diode laser, 30 mW) and emission band-pass filter (505 to 550 nm). A software tool (FRET Tool vs 5.0, Carl Zeiss) was used to map and quantify the FRET efficiency. Threshold values for the donor, acceptor, and FRET filter set, determined by averaging the fluorescence values of PE-NFC, were subtracted from all collected images as background fluorescence. PE-FLNFC (acceptor only) and PE-C30 + NFC (donor only) were used for measuring cross-talk in emission and bleed-through in excitation. For sensitized emission measurements, an output of 0.3% for the 405 nm laser and 1.1% for the 488 nm laser were used at 5× magnification. For acceptor photobleaching measurements, an output of 0.3% for 488 nm laser (44 s total bleaching time) and 0.5% for the 405 nm laser were used at 100× magnification.

SEM. A Zeiss Ultra 60 FE-SEM (Carl Zeiss Inc., Thornwood, NY) was used to collect SEM images of specimens. All SEM samples were sputter coated with 4 nm of Au/Pd (60 mass fraction %/40 mass fraction %) prior to SEM imaging. PE composites were cryo-fractured in liquid nitrogen prior to analysis.

Disclosure: This work was carried out by the National Institute of Standards and Technology (NIST), an agency of the U.S. government, and by statute is not subject to copyright in the United States. Certain commercial equipment, instruments, materials, services, or companies are identified in this paper in order to specify adequately the experimental procedure. This in no way implies endorsement or recommendation by NIST.

Acknowledgment. Financial support was provided by the National Institute of Standards and Technology and the Air Force office of Scientific Research under Award No. F1ATA00236G002.

Supporting Information Available: Photobleaching experiments; LSCM/FRET images. This material is available free of charge *via* the Internet at http://pubs.acs.org.

REFERENCES AND NOTES

1. Krishnamoorti, R. Strategies for Dispersing Nanoparticles in Polymers. *MRS Bull.* **2007,** *32*, 341–346.
2. Dzenis, Y. Structural Nanocomposites. *Science* **2008,** *319*, 419–420.
3. Schandler, L. Model Interfaces. *Nat. Mater.* **2007,** *6*, 257–258.
4. Vaia, R. A.; Liu, W.; Koerner, H. Analysis of Small-Angle Scattering of Suspensions of Organically Modified Montmorillonite: Implications to Phase Behaviour of Polymer Nanocomposites. *J. Polym. Sci., Part B: Polym. Phys.* **2003,** *41*, 3214–3236.

5. Zammarano, M.; Krämer, R. H.; Harris, R.; Ohlemiller, T. J.; Shields, J. R.; Rahatekar, S. S.; Lacerda, S.; Gilman, J. W. Flammability Reduction of Flexible Polyurethane Foams *via* Carbon Nanofiber Network Formation. *Polym. Adv. Technol.* **2008,** *19*, 588–595.
6. Morgan, A. B.; Gilman, J. W. Characterization of Polymer-Layered Silicate (Clay) Nanocomposites by Transmission Electron Microscopy and X-ray Diffraction: A Comparative Study. *J Appl. Polym. Sci.* **2003,** *87*, 1329–1338.
7. Li, Y. C.; Schulz, J.; Mannen, S.; Delhom, C.; Condon, B.; Chang, S. C.; Zammarano, M.; Grunlan, J. C. Flame Retardant Behavior of Polyelectrolyte-Clay Thin Film Assemblies on Cotton Fabric. *ACS Nano* **2010,** *4*, 3325–3337.
8. Wagener, R.; Reisinger, T. J. G. A Rheological Method To Compare the Degree of Exfoliation of Nanocomposites. *Polymer* **2003,** *44*, 7513–7518.
9. Bourbigot, S.; Vanderhart, D. L.; Gilman, G. W.; Awad, W. H.; Davis, R. D.; Morgan, A. B.; Wilkie, C. A. Investigation of Nanodipsersion in Polystyrene−Montmorillonite Nanocomposites by Solid-State NMR. *J. Polym. Sci., Part B: Polym. Phys.* **2003,** *41*, 3188–3213.
10. Graff, R. A.; Swanson, J. P.; Barone, P. W.; Baik, S.; Heller, D. A.; Strano, M. S. Achieving Individual-Nanotube Dispersion at High Loading in Single-Walled Carbon Nanotube Composite. *Adv. Mater.* **2005,** *17*, 980.
11. Maupin, P. H.; Gilman, J. W.; Harris, R. H.; Bellayer, S.; Bur, A. J.; Roth, S. C.; Murariu, M.; Morgan, A. B.; Harris, J. D. Optical Probes for Monitoring Intercalation and Exfoliation in Melt-Processed Polymer Nanocomposites. *Macromol. Rapid Commun.* **2004,** *25*, 788–792.
12. Kashiwagi, T.; Fagan, J.; Douglas, J. F.; Yamamoto, K.; Heckert, A. N.; Leigh, S. D.; Obrzut, J.; Du, F.; Gibson, S. L.; Mu, M.; Winey, K. Y.; Haggenmueller, R. Relationship between Dispersion Metric and Properties of PMMA/SWNT Nanocomposites. *Polymer* **2007,** *48*, 4855–4866.
13. Yoonessi, M.; Toghiani, H.; Daulton, T. L.; Lin, J. S.; Pittman, C. U. Clay Delamination in Clay/Poly(dicyclopentadiene) Nanocomposites Quantified by Small Angle Neutron Scattering and High-Resolution Transmission Electron Microscopy. *Macromolecules* **2005,** *38*, 818–831.
14. Thomas, C. I.; Lowe, R. M.; Ragauskas, A. J. Deformation Behavior of Wet Lignocellulosic Fibers. *Carbohydr. Polym.* **2007,** *69*, 799–804.
15. Bellayer, S.; Gilman, J. M.; Eidelman, N.; Bourbigot, S.; Flambard, X.; Fox, D. M.; DeLong, H. C.; Troulove, P. C. Preparation of Homogeneously Dispersed Multiwalled Carbon Nanotube/Polystyrene Nanocompolsite *via* Melt Extrusion Using Trialkyl Imidazolium Compatibilizer. *Adv. Funct. Mater.* **2005,** *15*, 910–916.
16. De Schryver, F. C. Time, Space and Spectrally Resolved Photochemistry from Ensembles to Single Molecules. *Pure Appl. Chem.* **1998,** *70*, 2147–2156.
17. Rittingstein, P.; Priestley, R. D.; Broadbelt, L. J.; Torkelson, J. M. Model Polymer Nanocomposites Provide an Understanding of Confinement Effects in Real Nanocomposites. *Nat. Mater.* **2007,** *6*, 278–282.
18. Giridharagopal, R.; Ginger, D. G. Characterizing Morphology in Bulk Heterojunction Organic Photovoltaic Systems. *J. Phys. Chem. Lett.* **2010,** *1*, 1160–1169.
19. Ajayan, P. M.; Braun, P.; Schadler, L. S. *Nanocomposite Science and Technology*; Wiley-VCH: Weinheim, Germany, 2003.
20. Needleman, A.; Borders, T. L.; Brinson, L. C.; Flores, V. M.; Schadler, L. S. Effect of Interphase Region on Debonding of a CNT Reinforced Polymer Nanocomposites. *Compos. Sci. Technol.* **2010,** *70*, 2207–2215.
21. Roth, C. B.; McNerny, K. L.; Jager, W. F.; Torkelson, J. M. Eliminating the Enhanced Mobility at the Free Surface of Polystyrene: Fluorescence Studies of the Glass Transition Temperature in Thin Bilayer Films of Immiscible Polymers. *Macromolecules* **2007,** *40*, 2568–2574.
22. Labardi, M.; Prevosto, D. Local Dielectric Spectroscopy of Nanocomposites Materials Interfaces. *J. Vac. Sci. Technol., B* **2010,** *28*, C4D11–C4D17.
23. Priestley, R. D.; Ellison, C. J.; Broadbelt, L. J.; Torkelson, J. M. Structural Relaxation of Polymer Glasses at Surfaces, Interfaces, and In Between. *Science* **2005,** *309*, 456–459.
24. Rittigstein, P.; Torkelson, J. M. Polymer−Nanoparticle Interfacial Interactions in Polymer Nanocomposites: Confinement Effects on Glass Transition Temperature and Suppression of Physical Aging. *J. Polym. Sci., Part B: Polym. Phys.* **2006,** *44*, 2935–2943.
25. Roy, M.; Nelson, J. K.; MacCrone, R. K.; Schadler, L. S. Polymer Nanocomposite Dielectrics—The Role of the Interface. *IEEE Trans. Dielectr. Electr. Insul.* **2005,** *12*, 629–643.
26. Ciprari, D.; Jacob, K.; Tannenbaum, R. Characterization of Polymer Nanocomposite Interphase and Its Impact on Mechanical Properties. *Macromolecules* **2006,** *39*, 6565–6573.
27. Kashiwagi, T.; Du, F.; Douglas, J. F.; Winey, K. I.; Harris, R. H.; Shields, J. R. Nanoparticle Networks Reduce the Flammability of Polymer Nanocomposites. *Nat. Mater.* **2005,** *4*, 928–933.
28. Förster, T. Intermolecular Energy Migration and Fluorescence. *Ann. Phys.* **1948,** *2*, 55–75.
29. Lakowicz, J. R. Energy Transfer. *Principles of Fluorescence Spectroscopy*, 3rd ed.; Springer: New York, 1999; pp 443−506.
30. Valuer, B. *Molecular Fluorescence: Principles and Applications*; Wiley-VCH: Weinheim, Germany, 2002; pp 247−272.
31. Abbe, E. Beiträge zur Theorie des Mikroskops und der Mikroskopischen Wahrnehmung. *Arch. Mikroskop. Anat.* **1873,** *9*, 413–468.
32. Paul, D. R.; Robeson, L. M. Polymer Nanotechnology: Nanocomposites. *Polymer* **2008,** *49*, 3187–3204.
33. Siro, I.; Plackett, D. Microfibrillated Cellulose and New Nanocomposite Materials: A Review. *Cellulose* **2010,** *17*, 459–494.
34. Zimmermann, T.; Bordeanua, N.; Struba, E. Properties of Nanofibrillated Cellulose from Different Raw Materials and Its Reinforcement Potential. *Carbohydr. Polym.* **2010,** *79*, 1086–1093.
35. Berney, C.; Danuser, G. FRET or No FRET: A Quantitative Comparison. *Biophys. J.* **2003,** *84*, 3992–4010.
36. Champion, J. V.; Meeten, G. H.; Senior, M. Optical Turbidity and Refraction in a Dispersion of Sperical Colloidal Particles. *J. Chem. Soc., Faraday Trans. 2* **1979,** *75*, 184–188.
37. Bellayer, S.; Gilman, J. W.; Eidelman, N.; Bourbigot, S.; Flambard, X.; Fox, D. M.; De Long, H. C.; Trulove, P. C. Preparation of Homogeneously Dispersed Multiwalled Carbon Nanotube/Polystyrene Nanocomposites *via* Melt Extrusion Using Trialkyl Imidazolium Compatibilizer. *Adv. Funct. Mater.* **2005,** *15*, 910–916.
38. Xia, Z.; Liu, Y. Reliable and Global Measurement of Fluorescence Resonance Energy Transfer Using Fluorescence Microscopes. *Biophys. J.* **2001,** *81*, 2395–2402.
39. Gordon, G. W.; Berry, G.; Liang, X. H.; Levine, B.; Herman, B. Quantitative Fluorescence Resonance Energy Transfer Measurements Using Fluorescence Microscopy. *Biophys. J.* **1998,** *74*, 2702–2713.
40. Youvan, D. C.; Silva, M.; Bylina, E. J.; Coleman, W. J.; Dilworth, M. R.; Yang, M. M. Calibration of Fluorescence Resonance Energy Transfer in Microscopy Using Genetically Engineered GFP Derivatives on Nickel Chelating Beads. *Biotechnology et alia* **1997,** *3*, 1–18.
41. Roche, E.; Chanzy, H. Electron Microscopy Study of the Transformation of Cellulose I into Cellulose III_I in Valonia. *Int. J. Macromol.* **1981,** *3*, 201–206.
42. Schermelleh, L.; Heintzmann, R.; Leonhardt, H. A Guide to Super-Resolution Fluorescence Microscopy. *J. Cell. Biol.* **2010,** *190*, 165–175.
43. Pertsinidis, A.; Zhang, Y.; Chu, S. Subnanometre Single-Molecule Localization, Registration and Distance Measurements. *Nature* **2010,** *466*, 647–653.
44. Helbert, W.; Chanzy, H.; Husum, T. L.; Schülein, M.; Steffen, E. Fluorescent Cellulose Microfibrils as Substrate for the Detection of Cellulose Activity. *Biomacromolecules* **2003,** *4*, 481–487.